

Raman Mapping Devoted to the Phase Transformation and Strain Analysis in Si Micro-Indentation

By F. Demangeot,* P. Puech, V. Domnich, Y. G. Gogotsi, S. Pinel, P. S. Pizani, and R. G. Jasinevicius

Micro-indentation testing is a standard technique for hardness measurements. Due to small size of the contact loading area, extremely high pressures can be produced within a confined zone on a material surface. It is well known that Si undergoes a semiconductor/metal transition at a hydrostatic pressure of ~12 GPa with the metallic Si-II phase transforming into various Si polymorphs up on depressurization.^[1,2,3] In indentation testing, the transition path of Si on Load release depends significantly on the unloading rates used: crystalline Si-III (body-centered cubic structure, *bc8*) and Si-XII (rhombohedral structure, *r8*) polymorphs are observed after slow load release, whereas rapid unloading leads to the formation of amorphous material (*α*-Si) in the affected zone.^[4] Additionally, strain and stress in (*cd*) Si has received attention, both from a theoretical and experimental point of view.^[5-7] Raman spectroscopy is a valuable tool to address these two questions. This non-destructive technique can be used to probe different phases by selective tuning between excitation energy and fundamental electronic transition energy of the associated phases.^[8] In depth information can also be gained thanks to the use of several excitation wavelengths. In addition, the possibility to achieve high spectral (~0.1 meV) and spatial (~1μm²) resolution makes Raman microspectroscopy an ideal tool to quantitatively study the spatial distribution of the strain around indentations in Si.^[9]

[*] Dr. F. Demangeot, Dr. P. Puech
Laboratoire de Physique des Solides
Université Paul Sabatier,
31062 Toulouse Cédex (France)
Dr. V. Domnich, Prof. Y. G. Gogotsi
Department of Materials Engineering
Drexel University, Philadelphia PA 19104 (USA)
S. Pinel
Laboratoire d'Analyse et d'Architecture des Systèmes
UPR 8001 CNRS, Avenue du Colonel Roche
31077 Toulouse Cédex (France)
P. S. Pizani
Departamento de Física
Universidade Federal de Sao Carlos
13565-970 Sao Carlos (Brazil)
R. G. Jasinevicius
Universidade de Sao Paulo
Escola de Engenharia de Sao Carlos
C. P. 369, 13560-970 Sao Carlos (Brazil)

In this paper, we briefly describe the theory of strain induced frequency shift. We show that accurate 2D Raman imaging can be used to map the three dimensional strain field around a micro-indentation and to deduce the extension of the plastic deformation. Then, the spatial distribution of strain and phases in several nano-indentations produced under different loads is analysed by 1D Raman mapping, which furnishes all the relevant information. The obtained strain profile of the Berkovich indentation is discussed.

A single peak associated with the triply degenerate Γ_{15} long wavelength optical phonons is observed in the Raman spectrum of crystalline silicon (cubic diamond structure), in the absence of strain. In a strained crystal, the symmetry is lowered and the diagonalisation of the modulation of the dynamical matrix gives the frequency shifts and the polarisation of the phonon.^[10]

Assuming that the stress tensor has a diagonal form^[10] in the XYZ basis for (001)-oriented sample (X, Y, and Z are chosen along $[1\bar{1}0]$, $[110]$, and $[001]$ respectively);

$$\sigma = \begin{pmatrix} \sigma_{\parallel} & 0 & 0 \\ 0 & \sigma_{\parallel} & 0 \\ 0 & 0 & \sigma_{\perp} \end{pmatrix} \quad (1)$$

where σ_{\perp} represents the stress component along the $[001]$ direction and σ_{\parallel} is the stress component in the surface plane. Based on the phonon deformation potential theory, the induced frequency shifts in cm⁻¹ are given by:^[11,12]

$$\begin{aligned} \Delta\omega_S &= -3.7 \sigma_{\parallel} - 0.44 \sigma_{\perp} \\ \Delta\omega_D &= -2.3 \sigma_{\parallel} - 1.84 \sigma_{\perp} \end{aligned} \quad (2)$$

where S stands for singlet (atoms motions along the Z direction) and D for doublet (atoms motions perpendicular to the Z direction). The strain element tensors are related to the stress tensor elements through the compliance tensor as follows;

$$\begin{pmatrix} \epsilon_{\parallel} \\ \epsilon_{\perp} \end{pmatrix} = \begin{pmatrix} S_{11} + S_{12} & S_{12} \\ 2S_{12} & S_{11} \end{pmatrix} \begin{pmatrix} \sigma_{\parallel} \\ \sigma_{\perp} \end{pmatrix} = \begin{pmatrix} 5.54 \cdot 10^{-3} & -2.14 \cdot 10^{-3} \\ -4.28 \cdot 10^{-3} & 7.68 \cdot 10^{-3} \end{pmatrix} \begin{pmatrix} \sigma_{\parallel} \\ \sigma_{\perp} \end{pmatrix} \quad (3)$$

The Raman intensity is deduced from the following equation:

$$I = \sum_{\Delta} \left\{ \left| \sum_{\alpha\beta} \vec{e}_{i\alpha} \vec{e}_{s\beta} \Gamma_{15\alpha\beta}(\Delta) \right|^2 L(\omega_{\Delta}) \right\} \quad (4)$$

where \vec{e}_i and \vec{e}_s are the incident and the scattered photon polarization, and $L(\omega)$ is the Lorentzian response of the phonon. In the basis XYZ, we have the following Γ_{15} tensors;

$$\begin{aligned} \Gamma_{15}(X) &= d \begin{bmatrix} 0 & 0 & -1 \\ 0 & 0 & 0 \\ -1 & 0 & 0 \end{bmatrix}, \Gamma_{15}(Y) = d \begin{bmatrix} 0 & 0 & 0 \\ 0 & 0 & 1 \\ 0 & 1 & 0 \end{bmatrix}, \\ \Gamma_{15}(Z) &= d \begin{bmatrix} -1 & 0 & 0 \\ 0 & 1 & 0 \\ 0 & 0 & 0 \end{bmatrix} \end{aligned} \quad (5)$$

which symmetries determine the Raman selection rules. If \vec{e}_i and \vec{e}_s are collinear, for example along X, we select the tensor element $\Gamma_{15XX}(Z)$ which corresponds to atoms moving along Z. In crossed configuration, there is no Raman intensity allowed. However, in a preceding work,^[13] we have shown that in crossed configuration and back-scattering geometry along (001), all tensors contribute to the low intensity when some disorientation take place.

The optical image of the micro-indentation after polishing is shown in Figure 1. First, we tested the effect of annealing. Figure 2 shows the Raman spectra from the center of the indentation, recorded with various laser powers. The time-power product was kept constant for these experiments. Amorphous phase (α -Si) is assigned in every spectrum by a broad band centered at $\sim 470 \text{ cm}^{-1}$.^[16] More interesting is the fact that we observed up to three peaks located at $\sim 516 \text{ cm}^{-1}$ (511 in crossed polarization), 522 cm^{-1} and 530 cm^{-1} . These peaks may be assigned to Si-IV, unstrained Si-I and Si-I under

compressive strain.^[4] Alternatively, the peak at 516 cm^{-1} may be attributed to the presence of nanocrystalline material in the indentation contact area.^[16]

To produce the map in Figure 3, we recorded the spectra in crossed and parallel polarization configuration. In parallel configuration, the spectrum reveals only one peak shifted by 6.45 cm^{-1} from the reference, corresponding to the single component. In the crossed configuration, where no Raman activity is allowed in a perfect crystal, we observe two peaks (singlet and doublet) located at 6.45 cm^{-1} and 3 cm^{-1} from the reference, leading to $\sigma_{\parallel} = -1.8$ and $\sigma_{\perp} = +0.6 \text{ GPa}$ (Eq. 2), and to $\epsilon_{\parallel} = -12 \cdot 10^{-3}$ and $\epsilon_{\perp} = +13 \cdot 10^{-3}$ (Eq. 3). In these cases, the conversion factor between the frequency shift and the stress is chosen to be $-3.2 \text{ cm}^{-1}/\text{GPa}$ for σ_{\parallel} as proposed by E. Anastassakis et al.^[17] We have approximately $\epsilon_{\parallel} \simeq -\epsilon_{\perp}$ and $\Delta\omega_S \simeq -500 \epsilon_{\parallel}$, and we use this last equality to produce the 2D-map of the silicon phonon shift presented in Figure 3. Even if the shift is almost invariant to rotation around the Z axis, one can still observe some darker crossed lines, which indicates that some stress relaxation took place along the cracks, as evidenced in Figure 1. Notice that the product $r \cdot \Delta\omega$ is nearly constant ($25 \mu\text{m} \cdot \text{cm}^{-1}$) when r varies from 0 to $20 \mu\text{m}$. By using Equation 6, we deduce that the strain approximately follows the relation $\epsilon_{\parallel} = -\langle E0.055 \cdot r(\mu\text{m}) \rangle$ in the volume of the indentation.

We now proceed to the discussion of the results obtained on Berkovich nano-indentations. An array nanoindentations corresponding to different maximum loads and loading/unloading rates was produced (Fig. 4). The size of the residual impressions ranges from $3.5 \mu\text{m}$ (for 100 mN load, observed in the center of the figure) to $1.5 \mu\text{m}$ (30 mN load).

Figure 5a shows the Raman spectra acquired along the line crossing 100 mN load indent. First, a maximum shift of 6 cm^{-1} is observed between spectra separated at $5 \mu\text{m}$, corresponding to the following value for the strain: $\epsilon_{\parallel} = -1.2 \cdot 10^{-2}$.

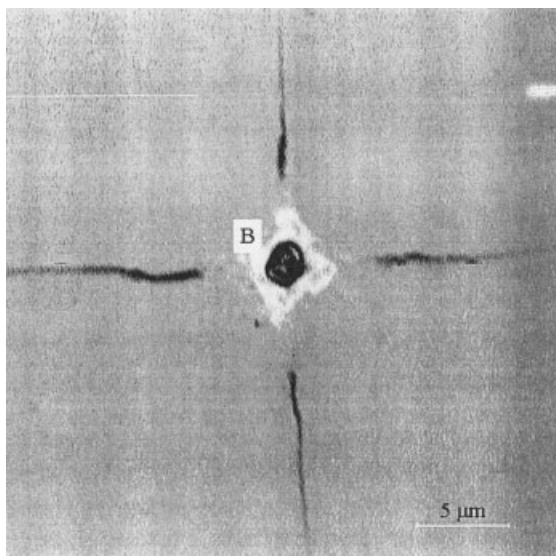


Fig. 1. Optical images of the indentation after abrasive chemical polishing.

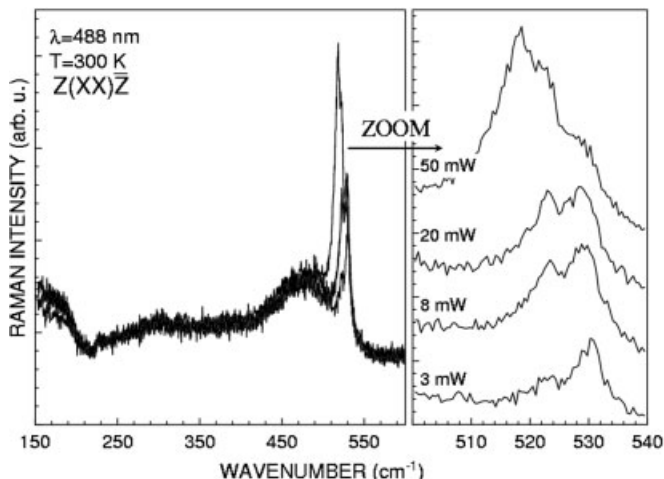


Fig. 2. Effect of partial annealing in the center of the indentation. The product power of illumination - time of accumulation is kept constant.

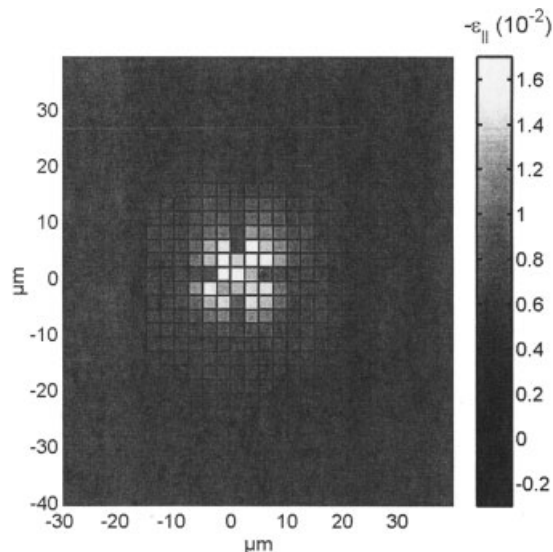


Fig. 3. Transverse deformation ($-\epsilon_{\parallel} = \Delta\omega/500$) in the indentation after abrasive chemical polishing.

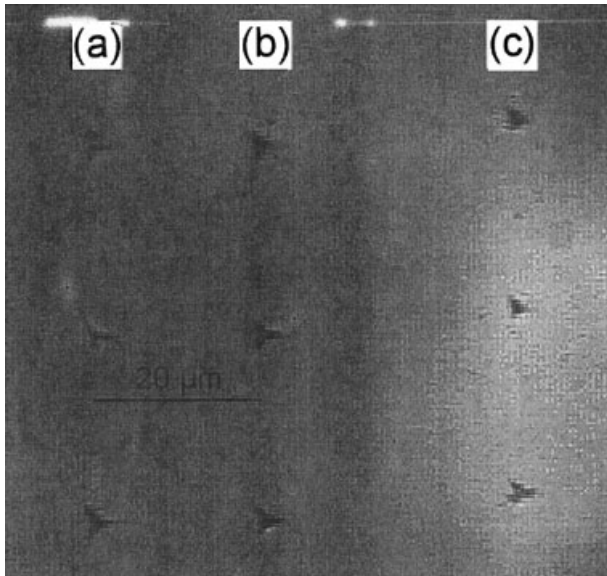


Fig. 4. Optical image of the Berkovich nano-indentations. Indentations of the column a) and b) have been both produced with 100 mN loads and with loading rates of 0.3 mN for column a) and 1 mN for column b).

From Figure 5b, several signatures are obtained in the 300–500 cm^{-1} range, revealing the presence of metastable Si phases (modes at 353, 384, 397, 415, and 434 cm^{-1} associated with the Si-III and Si-XII) and amorphous silicon (broad band centered at $\sim 470 \text{ cm}^{-1}$).^[16] Careful analysis of all these phases is beyond the scope of this paper. We note here that only amorphous Si was revealed by Raman spectroscopy in Vickers micro-indentation (1N) produced under rapid unloading rate, in accordance with previous observations. Also, varying the excitation wavelength revealed additional Raman bands at 378 cm^{-1} and 420 cm^{-1} , which may be attributed to the Si-XII phase, and a band at 322 cm^{-1} , which origin is not entirely understood at this time.^[16]

The two next maps show strong correlation between the spatial distribution of the metastable Si phases and the strain in the surrounding (cd)-Si. The intensity ratio (350 cm^{-1} / 520 cm^{-1}) is plotted as a function of the position of the laser spot with respect to the two 100 mN load indents, shown in Figure 6. This profile suggests that the metastable r8 and bc8 phases are inversely correlated to the presence of (cd)-Si. The relative amount of the metastable phases is higher for a 100 mN/s indent because the area of the transformed zone is larger in this case. The effect of the loading rate on the volume of the metastable phases has been confirmed on other indentations.

This profile can be compared with the strain profile through the indents, designed in Figure 7. Maximum strain lies near the center of the triangular impression, which correlates with the maximum content of the metastable Si phases (Fig. 6). However, it should be taken into account that the size of the nano-indentations is comparable with that of a laser spot, and hence the apparent increase in the degree of transformation towards the indentation center may be attributed to a decrease in the contribution of the surrounding Si-I to the

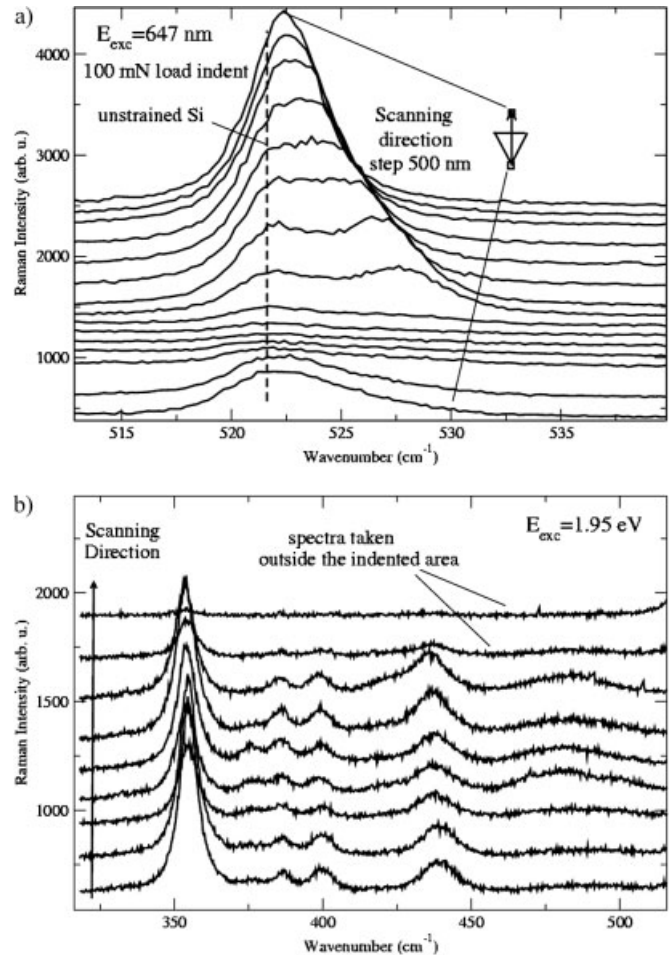


Fig. 5. Raman spectra from different locations with respect to the 100 mN indentations. (cd)-Si Raman mode through the indented area. Vibration modes of Si polymorphs.

overall Raman response. Notice the asymmetry of the profile in Figure 7. The strain variation is very strong in the direction defined by two facets (observed on the two indents), while this variation is not so pronounced in the direction perpendicular to the third facet. It is well known that various types of extended cracks may form during the indentation test. Our

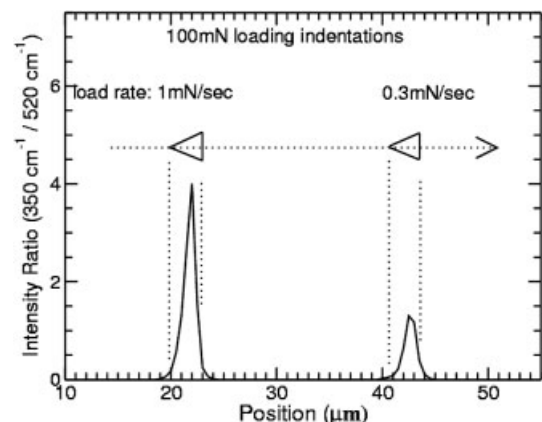


Fig. 6. Line scan of relative intensity of r8/bc8 Si peak at 350 cm^{-1} across the indentations.

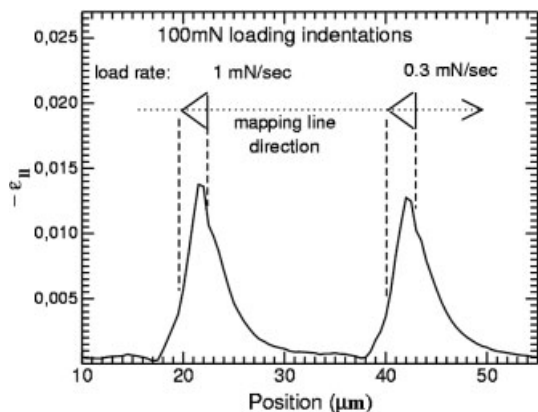


Fig. 7. Strain distribution across the indentations ($-\epsilon_{||} = \Delta\omega/500$).

work suggests that these cracks, which are taken as responsible for the large stress relaxation on one side of the indent, are mainly induced by the shape of the indenter, in our case the three edges of the pyramid. From this strain variation, we extracted at least one region where the strain varies as $(1/r)$. This area extends only some 3–5 μm outside the indentation contact area, which is much smaller than in the case of a large micro-indentation. This suggests a direct correlation between the applied load and the dimension of the plastic deformation zone.

Experimental

The Vickers indentation was produced by applying 1 N load for 15 s at room temperature on a (001) silicon surface, followed by a rapid unloading. The 2 μm -thick layer has been removed using an alkaline colloidal silica abrasive solution (Syton). This way, no disorder is introduced into the surface layer affected during contact loading.^[14] Nano-indentation tests were performed on a Nano Indenter[®] XP (MTS) tester using a Berkovich pyramid, with maximum loads ranging from 30 to 100 mN and loading rates from 1 to 3 mN/s. The same rates were used for loading and unloading.^[15]

Raman measurements were performed at room temperature in back-scattering geometry with parallel polarization using an XY Dilor spectrometer at several excitation wavelengths of an (Ar^+ , K^+) laser ranging from 476 nm to 647 nm. The Raman spectra presented here were recorded with a 10 s exposure and a 0.5 μm step by using an automatized XY table coupled to the spectrometer. Total acquisition times for both a 2D map and a 1D line map did not exceed 2 hours. The laser intensity was focused with a high numerical aperture objective (N.A. ~ 0.95) leading to a 1 μm^2 illuminated area. The Raman probe depth was 0.5 μm for 476 nm and 2 μm for 647 nm excitation.^[12]

Received: May 01, 2002

[1] R. J. Needs, A. Mujica, *Phys. Rev. B* **1995**, *51*, 9652.
 [2] R. O. Piltz, J. R. Maclean, S. J. Clark, G. J. Ackland, P. D. Hatton, J. Crain, *Phys. Rev. B* **1995**, *52*, 4072.
 [3] J. Crain, G. J. Ackland, J. R. Maclean, R. O. Piltz, P. D. Hatton, G. S. Pawley, *Phys. Rev. B* **1994**, *50*, 13043.
 [4] A. Kailer, Y. G. Gogotsi, K. G. Nickel, *J. Appl. Phys.* **1997**, *81*, 3057.
 [5] J. S. Kallman, W. G. Hoover, C. G. Hoover, A. J. De Groot, S. M. Lee, F. Wooten, *Phys. Rev. B* **1993**, *47*, 7705.
 [6] M. Yoshioka, *J. Appl. Phys.* **1994**, *76*, 7790.
 [7] K. Minowa, K. Sumino, *Phys. Rev. Lett.* **1999**, *69*, 320.

[8] V. Paillard, P. Puech, M. A. Laguna, P. Temple-Boyer, B. Caussat, J. P. Couderc, B. De Mauduit, *Appl. Phys. Lett.* **1998**, *73*, 1718.
 [9] P. Puech, S. Pinel, R. G. Jasinevicius, P. S. Pisani, *J. Appl. Phys.* **2000**, *88*, 4582.
 [10] E. Anastassakis, *J. Appl. Phys.* **1999**, *86*, 249.
 [11] F. Cerdeira, C. J. Buchenauer, F. H. Pollak, M. Cardona, *Phys. Rev. B* **1972**, *5*, 580.
 [12] A. De Wolf, *Semicond. Sci. Technol.* **1996**, *11*, 139.
 [13] P. Puech, E. Daran, G. Landa, R. Carles, P. S. Pisani, C. Fontaine, *J. Appl. Phys.* **1995**, *77*, 1126.
 [14] S. Pinel, J. Tasselli, J. P. Bailbe, A. Marty, P. Puech, D. Esteve, *J. Micromech. Microeng.* **1998**, *8*, 338.
 [15] V. Domnich, Y. G. Gogotsi, S. Dub, *Appl. Phys. Lett.* **2000**, *76*, 2214.
 [16] V. Domnich, Y. G. Gogotsi, in: *Handbook of Surfaces and Interfaces of Materials* (Ed. H. Nalwa), Vol. 2, Ch. 5, Academic Press, **2001**.
 [17] E. Anastassakis, E. Liarokapis, *J. Appl. Phys.* **1987**, *62*, 3346.

Electronic Speckle Pattern Interferometry for Micromechanical Measurements

By Sigitas Tamulevičius,* Lindas Augulis, Giedrius Laukaitis, and Marius Žadvydas

Electronic Speckle Pattern Interferometry (ESPI) (or TV Holography) combines different aspects and properties typical for the optical interference and holographic methods.^[1,2] In this method a complicated interference fringe pattern due to interference between the waves reflected from the reference and measured surfaces is registered in a limited aperture optical system. Areas of correlated motion of the surface are used to define tangential or normal (out of plane) displacement due to vibration, thermal or mechanical exposure of the subject. Application of the different type of optical schemes allows to define 3D measurements.^[3,4] Diverse applications of ESPI including^[5,6] studies of thin films mechanical properties were reported. Data acquisition and analysis is performed in real time, so this method becomes versatile for in-situ measurements. On the other hand, most of the methods reported are focused on the measurements on objects with typical linear dimensions much bigger than 1 mm,

*] Dr. S. Tamulevičius, Dr. L. Augulis, Dr. G. Laukaitis, Dr. M. Žadvydas
 Department of Physics
 Kaunas University of Technology
 Studentu 50, LT-3028, Kaunas (Lithuania)